SSC24-V-04

Demisability Investigation with the CubeSat SOURCE: Plasma Wind Tunnel Experiment Results

Daniel Galla, Clemens Kaiser, Iftekher Ahamed, Marco Siegle, Georg Herdrich, Sabine Klinkner
University of Stuttgart, Institute of Space Systems
Pfaffenwaldring 29, 70569 Stuttgart; +49 711 685 62313
galla@irs.uni-stuttgart.de

Kaja Gebhard, Paul Jannik Haufe, Philipp Hoffmann, Timon Jarothe, Marcel Liegibel, Michael O'Donohue
University of Stuttgart, Small Satellite Student Society
Pfaffenwaldring 29, 70569 Stuttgart
kaja.gebhard@ksat-stuttgart.de

ABSTRACT

The increasing utilization of small satellites in Low Earth Orbit (LEO) facilitates ground-breaking opportunities including telecommunication, Earth observation, gravimetry, Space Situation Awareness (SSA) and atmospheric science. However, it also creates a challenge for space debris mitigation and space traffic management. Current numerical tools predicting satellite demisability during uncontrolled atmospheric entry lack accurate models, hindering the estimation of component survivability which is needed for a sustainable growth in orbital commercialization. The University of Stuttgart's Institute of Space Systems, together with the small satellite student society KSat e.V., addresses this issue with an interdisciplinary satellite re-entry analysis. This includes in-situ measurements in the early phase of re-entry with the Stuttgart Operated University CubeSat of Evaluation and Education (SOURCE), a 3+ Unit CubeSat scheduled for launch in 2025. The payload contains sensors for pressure, temperature, heat flux and atomic oxygen measurements during the early phase of re-entry at altitudes above 130 km. Iridium communication ensures a ground station-independent data downlink. Furthermore, numerical simulations with SCARAB (Hyperschall Technologie Göttingen, HTG) and PICLas (University of Stuttgart, IRS) including analysis for free molecular and continuous flow regimes identify critical components and points of interest in the trajectory. The demisability analysis is completed with plasma wind tunnel experiments. The plasma wind tunnel used for the tests at the University of Stuttgart is PWK1, which utilizes the self-field magnetoplasmadynamic plasma generator RD5 to create high-enthalpy air flows relevant for re-entry emulation. Three distinct trajectory points at different altitudes have been identified as test environments for the component tests, where relevant demise processes take place according to the numerical simulation results. An 80 mm diameter heat flux-pitot pressure probe was used to characterize the high-enthalpy flow, which emulates stagnation point conditions of the discrete trajectory points with focus on mass specific enthalpy and total pressure. The following components were selected as potential hard-to-demise components of SOURCE: The S-Band antenna, magnetorquers, printed circuit boards, a Carbon Fibre Reinforced Polymer (CFRP) sandwich structure, titanium rods, a camera, and batteries. Moreover, an experiment was conducted with a mock-up of SOURCE including functioning sensor arrays in a very low enthalpy environment to verify and investigate the reaction time of the in-situ measurements. All experiments are monitored with a linear pyrometer, an infrared camera, thermocouples, a spectrometer and recorded with a 4k video camera. The measurement results are in good agreement with the numerical simulations for the S-Band antenna, camera and titanium rods but differ for the magnetorquers, CFRP sandwich structure and PCBs. In particular, PCBs are candidates for hard-to-demise components in satellites that require an improved model for numerical simulations. The sensor validation test is showing the expected results in sensor performance, according to preliminary analysis.

INTRODUCTION

In recent years, the popularity of satellites in Very Low Earth Orbit (VLEO) and Low Earth Orbit (LEO) increased exponentially: Between 2018 and 2023 more objects were sent to an orbit between 200 km and 1750 km than in the previous 60 years combined. In total, their count increased to over 23,000.[1] This "NewSpace" trend emerged due to falling prices for satellite bus development and launching, spurred in part by the development of the CubeSat standard. These nanosatellites are low-cost to manufacture and deploy but have operational constraints due to their size. In the

past, a significant number of CubeSats have failed on arrival due to lack of experience and testing, increasing space debris and collision risk.[2] Even though this number decreased in recent years, not only CubeSats but manmade space debris in general has rose significantly. Since 1999, the International Space Station had to perform more than 38 manoeuvres to avoid getting hit by debris.[3] A collision of spacecraft parts could even potentially lock humanity from accessing space completely if the resulting cloud of debris covers the entire Earth. For those reasons, it is compulsory to keep orbits free from out-of-service satellites and debris parts. To address this, the European Space Agency (ESA) updated their Space Debris Mitigation Requirements in 2023 in the aim for a zero debris charta: the disposal phase in LEO was reduced from 25 years to five years.[4]

While this will keep LEO cleaner, another issue arises: most satellites are not designed with demisability as a design driver. For those satellites as well as other debris sources, only accurate simulations can predict whether the re-entry will completely burn up all components. This is challenging, as many simulation algorithms are either specialised on simulating single particles or a continuous fluid stream. During a re-entry, the particle density is steadily increasing. Therefore, the resulting plasma is not in a steady state. The University of Stuttgart developed the PICLas tool to counter this. PICLas is able to cover the gap by combining multiple methods to simulate collisional plasma flows.[5] While this allows for precise predictions of the re-entry environment, PICLas does not allow detailed modelling of satellite disintegration. ESA's Spacecraft Atmospheric Re-Entry and Aerothermal Break-Up (SCARAB) tool developed by Hyperschall Technologie Göttingen GmbH (HTG) incorporates this technology, rendering it ideal for risk analysis of re-entry processes.[6] Still, as a basis for all simulation programs detailed material data is necessary, especially thermal-physical properties. Those are best obtained by experiments on material samples. The University of Stuttgart's Institute of Space Systems tested different materials in its plasma wind tunnels: Not only commonly used metallic alloys such as Ti-6Al-4V or high temperature ceramics, but also laminate composites were examined.[7] However, spacecraft are made of a combination of many different materials joined together with screws, glue or strings. For demising spacecraft, especially those joints are weak points of the structure, prone to break first. Tests on Composite Overwrapped Pressure Vessel (COPV) segments proved to be very insightful during the CHARDEM and CoDM studies: For example, it was observed that a "pouch" containing liquified material can form which later ruptures due to mechanical forces.[8,9] Similar tests on entire components were performed by ESA, Belstead Research Limited and the German Aerospace Center DLR: In the Spacecraft Equipment Characterisation in Re-Entry Tests (SECRET) typical spacecraft components like magnetorquers, a reaction wheel, an electronic box section, ball bearing units and batteries were tested for their demise in a plasma wind tunnel.[10] However, plasma wind tunnel tests can be only conducted on a limited number of steady-state points of a re-entry. By selecting those points beforehand through simulations, plasma wind tunnel tests are biased by the existing materials data.

The most accurate data can only be obtained from uncontrolled re-entries themselves. One approach is to observe spacecraft re-entries as it was done for the Jules Verne ATV-1 on September 29, 2008: the atmospheric burn-up was filmed from two aircrafts and the ISS.[11,12] Furthermore, observing ESA's AVUM and simulating points of the trajectory in plasma wind tunnel tests significantly enhanced R.Tech's PAMPERO simulation tool and HTG's SCARAB tool.[13] However, since not all environmental properties can be deducted from visual data, a further enhancement is to obtain data directly in-situ on the re-entering vehicle itself. This requires building a spacecraft for the purpose of re-entering. Nanosatellites like CubeSats are ideal for this as they can be developed quickly with a low-cost satellite bus. The Undergraduate Nano Ionospheric Temperature Explorer (UNITE) satellite developed by the University of Southern Indiana, which was equipped with a Langmuir plasma probe and a variety of temperature sensors, successfully re-entered the Earth's atmosphere on October 21, 2021.[14] Other satellites designed to observe their own re-entry were 'EntrySat' by the Institut Supérieur de l'Aéronautique et de l'Espace in Toulouse or 'SASSI2' by Purdue University and the University of Illinois. Both were launched on April 17, 2019, but did not survive until the critical re-entry phase.[15,16,17] Almost one year later, the QARMAN satellite, an ESA-funded project lead by the von Karman Institute of Fluid Dynamics (Belgium), was launched. After five months of operation, it stopped communicating before re-entering on February 5, 2022. It is believed that overheating lead to battery failure.[18] The University of Tokyo launched two satellites with deployable aeroshells: 're-Entry satellite with Gossamer aeroshell and GPS/iridium' (EGG) in 2017 and 'Breakthrough by

Egg-derived Aerocapture Kilt vehicle' (BEAK) in 2023 to investigate satellite re-entry. EGG successfully demonstrated its inflatable heat shield, which shielded the satellite during the re-entry.[19,20] As BEAK was launched only recently, it has not reached its re-entry phase yet. BEAK will not only control its attitude during re-entry but already after being launched by opening its external solar arrays with film stretched between them.[21]

To mitigate the risk and diversify the data sources, the University of Stuttgart's Institute of Space Systems (IRS) and the Small Satellite Student Society of the University of Stuttgart (KSat) started the Stuttgart Operated University CubeSat for Evaluation and Education (SOURCE) project: A CubeSat is being built, equipped with a variety of sensors to characterise its re-entry. Before the satellite is launched, simulations with the PICLas and SCARAB tools are performed. Additionally, plasma wind tunnel tests of single components as well as the whole satellite are conducted. This broad approach is therefore able to significantly enhance our understanding of re-entries.

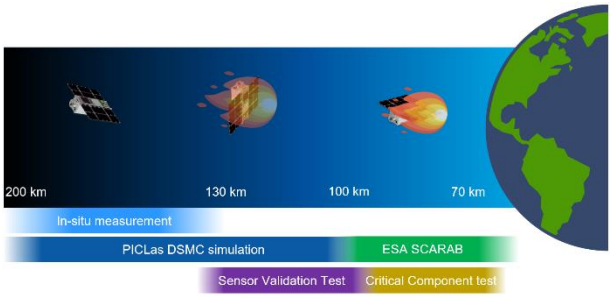

Figure 1: SOURCE interdisciplinary approach on satellite re-entry investigation

Figure 1 shows the distribution of data sources over the altitude of the satellite: Between 200 km and 100 km, PICLas simulations are complemented by in-situ data from SOURCE. Below 120 km, plasma wind tunnel tests and SCARAB simulations complete the data set.

This work will give an insight into the SOURCE project, its satellite bus and will present the interdisciplinary approach of the demisability analysis with a focus on plasma wind tunnel tests of hard-to-demise components and a satellite mock-up. Preliminary results will be shown, including non-intrusive and in-situ measurements during the plasma wind tunnel experiments, accompanied by a comparative analysis with numerical simulations.

THE CUBESAT SOURCE

SOURCE is a 3+ Unit CubeSat developed by KSat and IRS, both from the University of Stuttgart. Additionally, the project is supported by ESA's "Fly Your Satellite!" program with reviews and a launch opportunity 2025-26. Since the project started in 2018 over 400 graduate and undergraduate students together with PhD students have been working on designing, developing, and testing the satellite. One of its main mission goals is the education of the next generation of space engineers with hands-on experience.[22] The main scientific purpose, besides technology demonstration and meteor observation, is the investigation of re-entry events with in-situ measurements. Five sensor arrays consisting of pressure, temperature und heat flux sensors and additionally two atomic oxygen sensors collect data during the early phase of re-entry (200-130 km). A CAD model of the deployed SOURCE satellite is shown in Figure 2.

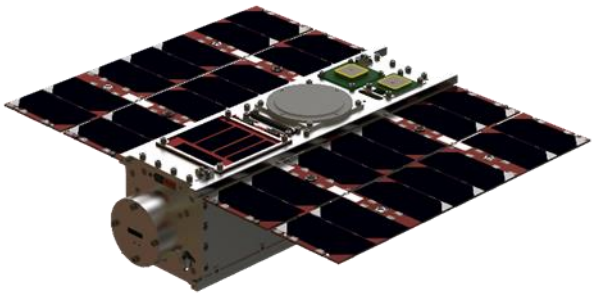

Figure 2: CAD of SOURCE in Orbit

Project Structure

The project team is separated into the eight following subsystems:

Attitude Control System (ACS), Communication (COM), Electrical Power System (EPS), Onboard Data Handling and Onboard Software (OBDH&OBSW), Operations and Ground (OPS&GND), Payload (PL), Structure and Thermal and Harness (Str&Th&H) and Simulation and Testbed (SIM&TB).

Each Subsystem with 8-10 students is supported by one or two PhD students. The project and the subsystem coordination are done in a management team consisting of student team leads, student system engineers and project coordinators from the institute. Thereby, students not only learn about the technical side of a satellite project but also about the management and organization part. The university also provides a one semester course, in which each student can earn credit for their studies. Many students use this course as a starting point in this

project. Since 2020, after SOURCE got accepted to the third round of the "Fly Your Satellite!" program, students can attend specialized courses at the ESA education center and teach the knowledge to the other students in the project. Moreover, dedicated ESA test facilities are usable by project members for component and system verification. Additionally, the KSat workshop and the clean room in the IRS provide workspaces with necessary tools for the project progression. The KSat workshop is mainly used for the development and testing of the components. Meanwhile, the clean room is used for the software development on the FlatSat (flat test setup of the satellite) as well as the Flight Model (FM) production and assembly.

Bus System

The dimensions of SOURCE are conformant with the CubeSat standard with 100 x 100 x 360 mm and it weighs about 4.3 kg. The main components of SOURCE are stacked along the z axis on four titanium threaded rods located in the corners. Figure 3 shows the CAD model of the stack, with the bus system components highlighted.

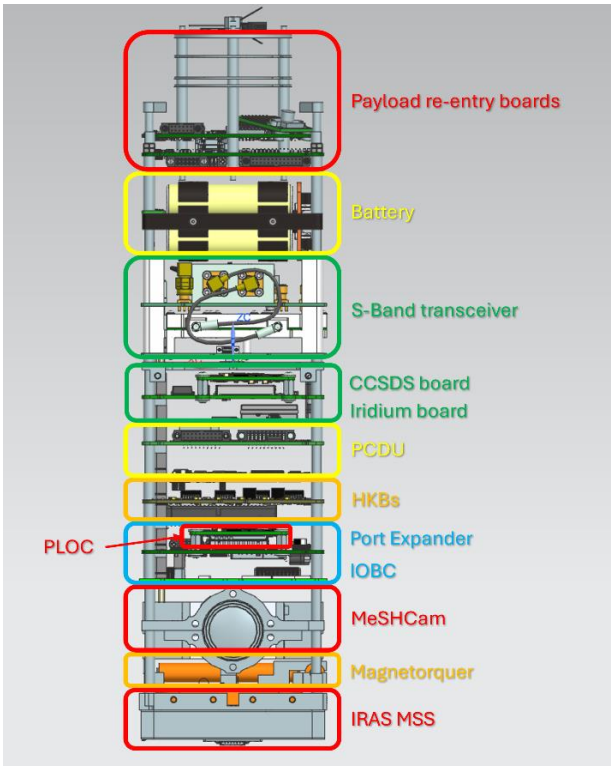

Figure 3: CAD model of stack with the components of each subsystem highlighted (purple: Payload, red: EPS, dark blue: COM, blue: ACS, green: OBDH&OBSW)

The majority of the electronic boards are stacked on a PC104 connector, starting with the Onboard Computer (OBC), located above the Meteor-, Star- and Horizontracking Camera (MeSHCam), and ending with the S-Band transceiver. Most of the Commercial of The Shelf (COTS) products use PC104, hence the self-developed boards were adapted accordingly. The data processing and handling is done by the onboard computer called IOBC, which was purchased from ISISpace. The software running on the IOBC is developed in-house and utilizes the Flight Software framework (FSFW) developed by IRS. The FSFW has been used successfully on the two previous missions Flying Laptop and EIVE from the University of Stuttgart and is updated and adjusted regularly.[23,24] The Payload subsystem uses a separate onboard computer called PLOC for the camera system, which processes the images and uses an algorithm to identify pictures with meteors.[25] This is done with a TE7020 by Trenz which is connected over an in-house developed port expander to the IOBC. The software running on the PLOC is based on the FSFW as well. The PLOC controls the two cameras installed on SOURCE. The MeSHCam is a COTS product by Teledyne DALSA as well as the PRIma, which is from ArduCam. The software for both cameras is developed and tested by students. Following on the stack, the two in-house produced housekeeping boards (HKBs) are used to convert analog temperature and sun sensor values to digital read-outs for the OBC. The determined attitude can be controlled via the self-developed and in-house manufactured magnetorquers. Next on the stack is the Power Control and Distribution Unit (PCDU), which was developed by the student team to meet the bus requirements on voltage and current. It consists of two printed circuit boards (PCBs), which can supply all systems with 3.3 V, 5 V or unregulated voltage. The battery is a BPX lithium-ion battery by GomSpace with a capacity of 86 Wh, which is charged via 56 solar cells. The solar cells are mounted on the deployable panels and can generate up to 32 W. For communication between SOURCE and the ground stations an S-band Syrlinks transceiver is primarily used. As a backup and for the re-entry phase Iridium antennas and transceivers are installed. The Iridium board, the CCSDS board and the transceivers, which are managed by the communication subsystem, are located on the PC104 stack as well. As for the payload besides re-entry analysis, one of the technology demonstrators onboard is a Multifunctional Sandwich Structure (MSS) from the Integrated Digital Research Platform for Affordable Satellites (IRAS) project by the German Aerospace

Centre (DLR) and Fraunhofer Institute is installed at the opposite end of the satellite's tuna can. It will analyze the structural properties of a 3D-printed carbon fiber infused polyether ether ketone structure with buzzer feedback. Additionally, two sensor setups consisting of RADFET, ADC and gyroscopes sensors are placed in the structure. In the structure around one of them, the material is infused with tungsten particles for radiation shielding. The effectiveness of the shielding and the degradation of the sensors over time is analyzed with this experiment.[26] Another payload for technology demonstration is a smart heater experiment by Airbus, which automatically regulates temperature without the need of a micro controller. It is located on the outside of the satellite like the third technology demonstration, which is a thin film photovoltaic solar cell experiment developed by the DLR.

Mission Overview

The mission of SOURE can be divided into two phases as shown in Figure 4 and is expected to last between one and two years.

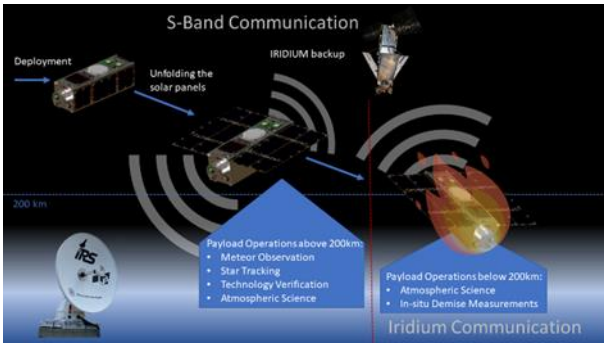

Figure 4: Mission Overview

In launch configuration, the solar panels are folded in twice to fit into the CubeSat dispenser. After the deployment, small Dyneema strings, which keep the panels in place, will be thermally cut and the solar panels are deployed by springs. In the first payload phase after commissioning, the camera system and technology demonstration payloads are operated. The MeSHCam is capturing black and white images of the earth during the eclipse. These images are being analyzed with the in-house developed meteor detection algorithm SpaceMEDAL and are intended to provide information about the quantity of re-entering meteors.[25] Additionally to meteor tracking, the MeSHCam can also be used to determine the attitude by tracking the stars and horizon. Moreover, PRIma pictures are captured as well for public outreach. Payloads from external partners are operated in this phase as well. During the first phase, the S-Band transceiver is used for communication with the ground station at the University of Stuttgart. The Iridium antennas for satellite communication are used as backup.

The second part of the SOURCE mission is the re-entry phase, which begins at an altitude of 200 km. During this phase, the re-entry sensors will analyze the impact of the atmosphere on the satellite. The data measured by the re-entry sensor system, which includes temperature, pressure, heat flux and atomic oxygen density, will be collected until the communication breaks off, most likely around 130 km. This data also includes attitude and tumbling rate during re-entry. During this phase, the ground station independent satellite communication service Iridium is used to obtain as much data as possible during descent.

Re-entry Sensor System

The re-entry sensor system consisting of the following four sensors:

1. PVC1004 by Posifa, a commercial pressure sensor
2. FM-120-K by Wuntronic, a commercial heat flux and temperature sensor
3. PHLUX developed at IRS, a heat flux sensor consisting of a coated and un-coated PT1000
4. FIPEX developed at IRS, an atomic oxygen sensor[27]

In total, five pressure, heat flux, temperature and PHLUX sensors as well as two of the FIPEX sensors will be analyzing the atmosphere from 200 km to around 130 km.[28,29]

The pressure sensor can measure from 0.1 Pa and 4000 Pa with a resolution of 0.6 Pa. The TO46 package of the PVC1000 was chosen, due to size constraints. It operates on the Pirani principle, which relates changes in pressure to variations in sensor resistance caused by temperature fluctuations. When the environmental pressure decreases and a current flows through a wire, the heat produced cannot transfer to the environment, causing the wire's temperature and resistance to increase. However, the temperature of the environment also increases as the pressure decreases. To account for this, a second wire is installed in the sensor and sealed from the environment, measuring only the changes in resistance due to environmental temperature variations.[31] The commercial sensors FM-120-K can measure temperature and heat flux. For the temperature measurement a nickel-chrome thermocouple (Type K) and for the heat flux measurement a copper-nickel thermopile (Type T) is used. Its heat flux range is

±9.5 kW/m^2 with a temperature range from −50 °C to 150 °C and an accuracy of ±5 %.[32]

The heat flux sensor PHLUX, developed in-house by the electric propulsion and plasma wind tunnel group at IRS, utilizes the different catalytic properties of two resistance thermometers. During re-entry, air molecules dissociate in the plasma in front of the satellite. Depending on the catalytic properties, the atoms recombine on the surface of the spacecraft in general and specifically on the two surfaces under investigation. The heat of formation released during the recombination is accommodated by the surface, leading to a temperature increase. The PHLUX sensor is utilized with two PT1000 resistance thermometers with materials of known catalytic characteristics to determine the catalytic heat flux. One PT1000 is coated with a highly catalytic material, increasing sensor temperature, while the other is left untreated and exposes the low catalytic Al_20_3 substrate to the flow. The temperature difference between both PT1000 sensors correlates with the atomic oxygen flux. To minimize heat flux conduction to the satellite structure, the sensors are thermally insulated with Airloy Aerogel.[33,34]

The in-house designed FIPEX sensors are 20 x 5 x 2 mm ceramic plates that have printed electrodes on one side. The electrodes are made from gold with a special electrolyte, which react with atomic oxygen when heated to 1000 K and creates a measurable current. Therefore, heating elements are printed to the other side of the ceramic plate. The Sensors are calibrated by the High Enthalpy Flow Diagnostics Group (HEFDiG) at IRS in an atomic oxygen environment.[27]

The re-entry sensors are assembled on an array, shown in Figure 5. This excludes FIPEX sensors, which are located in front and back of the satellite clamped on their holder.

Figure 5: Assembled sensor array with one pressure sensor and two heat flux sensors. From left to right: PVC1004, FM-120-K, PHLUX.

Figure 6 shows the placement of these sensor arrays along the CubeSat, including FIPEX sensors in purple. On position five, the pressure sensor is installed separate from the heat flux sensors due to the placement of the heat flux sensor in the IRAS MSS. The arrays on positions one to four are mounted to the side and top element from the inside, so that the surface area of the sensors is aligned with the surface of the structural elements. Equal alignment was done for the array on position five but to the surface of the IRAS MSS.

The Payload PCBs are placed in and close to the tuna can or SOURCE, marked blue in Figure 6. The two rectangle-shaped PCBs read out the data from the five sensor arrays including pressure, temperature and heat flux sensors. The radiation hardened microcontroller Vorago VA10820 controls the sensor data conversion and forward it to the OBC via RS485.[30] The measurement frequency can be varied up to a maximum of 1 Hz, limited by Iridium downlink capacity. The PCBs inside the tuna can are FIPEX PCBs operating the corresponding sensors. A radiation hardened microcontroller PIC24FJ1024GA606 (short: PIC24) was chosen due to heritage. It uses the RS485 Bus as well to communicate with the OBC.

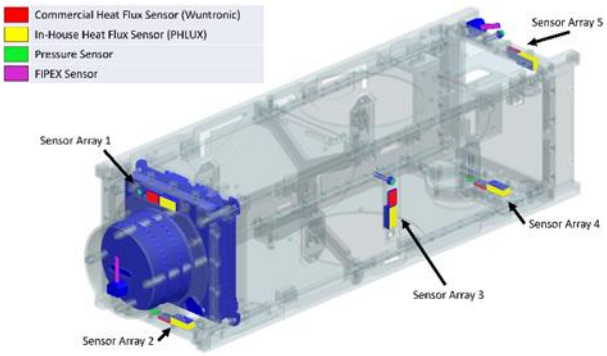

Figure 6: CAD Model of SOURCE with the re-entry system highlighted.

Current State of SOURCE

Currently, SOURCE is in phase D (manufacturing and testing) and completing the Manufacturing Readiness Review (MRR). Over the last year, all subsystem components with no flight heritage have successfully completed functional tests in a Thermal Vacuum Chamber (TVaC) under space conditions. The system wide vibration test was completed as well, completing the Qualification Model (QM) testing. Now, the focus is on the software development on a FlatSat (disassembled but connected QM/EM subsystems), shown in Figure 7, and the manufacturing of the FMs. Currently, 80 % of the components, which will be stacked in the CubeSat, are implemented on the flat sat

and connected to the other components. This allows the team to test their software with hardware in the loop. Communication tests between the OBC and different subsystem components, e.g. the payload boards, were already successful. Additionally, communication between OBC and the control room was achieved.

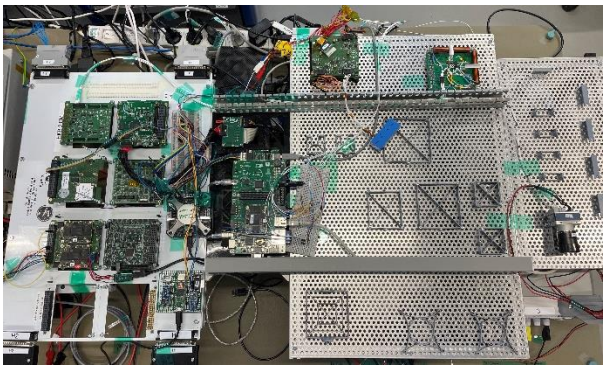

Figure 7: Current state of the flat sat in the IRS's clean room

EXPERIMENTAL DEMISE INVESTIGATION

As starting point for the in-situ demise investigation with SOURCE, simulations were done with PICLas for the early phase of re-entry between 200 km and 130 km. PICLas is a three-dimensional flow simulator, combining Particle-In-Cell (PIC), Direct Simulation Monte Carlo (DSMC), and other particle methods to simulate gas flows across various regimes. The framework has been validated for re-entry scenarios and extended for modeling polyatomic species in planetary atmospheres.[5] With this data, a sensor selection for the in-situ measurements was carried out and the design for the re-entry payload finalized.[35]

This is now followed by an experimental analysis in the plasma wind tunnel facilities at the University of Stuttgart. The IRS operates four plasma wind tunnels that can replicate the thermo-chemical conditions of the boundary layer near the stagnation point of re-entry bodies. Although the nitrogen-oxygen plasma flow within the plasma wind tunnel does not reach re-entry velocities, it can simulate the aerothermodynamic processes and heat flux density at the stagnation point for various trajectory points by adjusting the specific enthalpy, total pressure, and geometry. The test points for SOURCE's re-entry can be accurately reproduced regarding specific enthalpy and total pressure in PWK1 as illustrated by the CleanSpace CubeSat reference trajectory in Figure 8.[36] PWK1 is equipped with the magnetoplasma-dynamic arc plasma generator RD5.

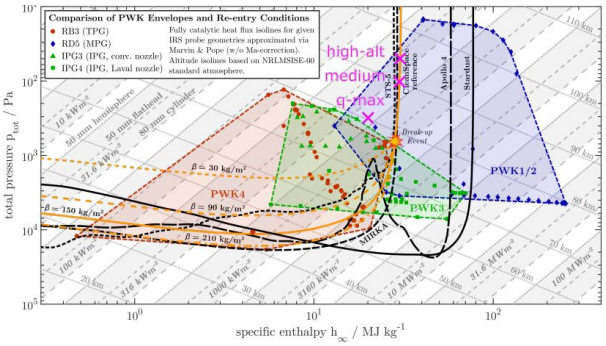

Figure 8: Operating ranges of the IRS plasma wind tunnels PWK1/2 (RD5), PWK3 (IPG3/4) and PWK4 (RB3) with example trajectories and the selected comparison points for the component tests[36]

In addition to the sensor validation in experimental environment, the plasma wind tunnel tests are used to investigate the demisability of SOURCE's components. This extends the interdisciplinary approach on satellite demise investigation even further by including the complete disintegration process as well. Especially the hard-to-demise components of the satellite are of interest, due to the risk of ground impact. To identify these, SCARAB simulations with different boundary conditions derived from possible trajectories were conducted. Moreover, these simulations determined the three main test conditions as shown in Table 1. Each condition represents a specific point of the calculated demise for a SOURCE component, also illustrated in Figure 8. For the test, suitable conditions in PWK1 are set using the control parameters gas mass flow, generator current, tank pressure, and probe position.[37]

In the following section, the setups for both the critical component test and the re-entry sensor validation are discussed.

Setup of the Critical Component Test

The critical component test focuses on the destructive analysis of specific satellite parts during re-entry. This is achieved by using the plasma wind tunnel to replicate the previously simulated re-entry conditions. To gain a better understanding of the demisability of SOURCE's components, the SCARAB simulations use a 3D-model of the entire satellite, which is numerically simulated for a complete re-entry with a dedicated orbit and correlating atmospheric conditions. These simulations are repeated with different orbital and atmospheric parameters suitable for the mission. This data set is then analyzed concerning enthalpy and stagnation pressure at the trajectory point of the component's demise or ground impact. From these results and in accordance with the

ESA Space Debris Mitigation Compliance Verification Guidelines[39], the following components are identified as potentially critical: the battery, the S-Band antenna, the IRAS-MSS, the payload PCBs, the magnetorquers, the MeSHCam, and the titanium threaded rods. [37,38]

These components are generally made of materials with high melting temperatures, making them less likely to completely burn up during atmospheric entry. Internal systems are considered more critical than exposed components, as they encounter direct atmospheric heating later. The three different test trajectory points, which can be seen as maxima in Figure 9, were prepared as conditions for the experimental setup.

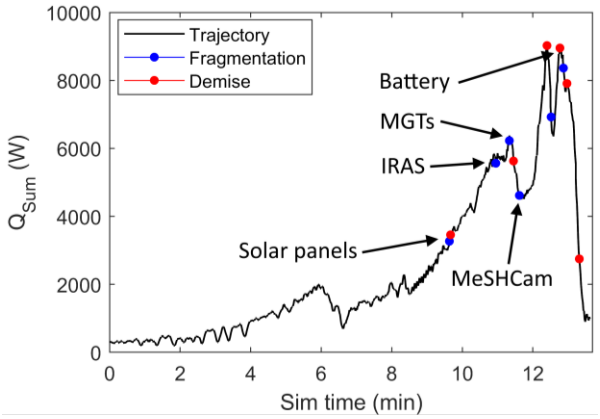

Figure 9: Simulated heat load for the critical part of re-entry with test trajectory points at 6, 11 and 13 minutes of simulation time

Parameter	Symbol	SRC-Ant	SRC-Med	SRC-Rod
total gas mass flow	$\dot{m}$ [g/s]	2.0	6.0	2.0
Tank pressure	p_{Tank} [Pa]	40	58	212
Total pressure	p_{tot} [Pa]	50	103	308
Heat flux density	$\dot{q}_{D=80\ mm}$ [kW/m^2]	195	275	329
Specific enthalpy (80mm ⌀ probe)	h [MJ/kg]	30.4	30.1	19.8
Generator current	I [A]	1200	1000	1200
Generator voltage	U [V]	66	85	66
position	x [mm]	520	515	570

Table 1: Operational parameters critical component test

The chosen operational parameters can be seen in Table 1. These were characterized by an 80 mm diameter heat flux probe. SRC-Ant represents a low heat flux demise event in the beginning, where the antenna is expected to experience a first significant increase in temperature. SRC-Med models the trajectory point where the satellite's main body starts to disintegrate, and the internals are exposed to the plasma. SRC-Rod represents the highest simulated heat flux environment during re-entry, where most of the components are expected to disintegrate. The full assignment of which component is tested at which point can be seen in the Table 2. It should be noted that the IRAS MSS was tested at SRC-Rod because previous experience already indicated deviations from SCARAB simulations. Consequently, it is expected that even the point of maximum heat flux in the experiments would not be sufficient for complete demise of IRAS MSS.

SRC-Ant	SRC-Med	SRC-Rod
S-Band Antenna	Magnetorquer	Titanium Rods
	MeSHCam	Payload PCBs
	Battery	IRAS-Sandwich
		MeSHCam-optics

Table 2: Assignment of components to trajectory points

For the test, each component is mounted on a brass water-cooled probe, and alignment with the plasma generator's beam center is ensured using a 3D line laser. Figure 10 shows this setup for a critical component, mounted on the probe and engulfed in the plasma beam.

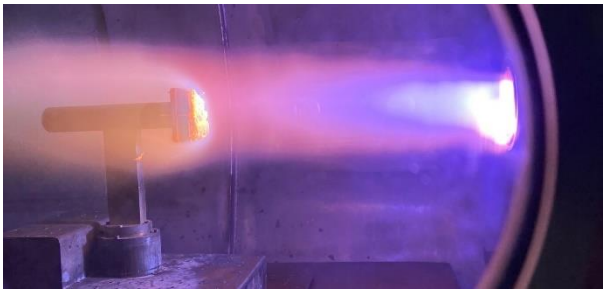

Figure 10: PCBs during their critical component test

Thermocouples attached with high-temperature adhesive Ceramabond 571 monitor temperature changes. In addition to contact-based temperature measurements, a FLIR A6751sc SLS thermographic imaging camera and an LP3 pyrometer are used to measure surface temperatures, as can be seen in the Figure 11.

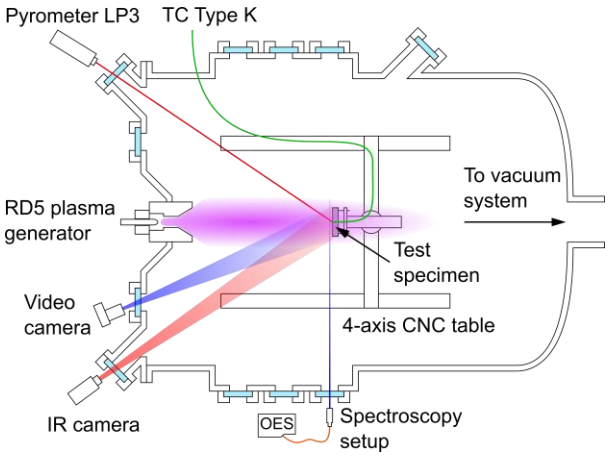

Figure 11: Setup of the critical component test

After the setup is successfully completed, the test component is positioned outside the plasma beam using a 4-axis CNC table. The chamber is then evacuated to a pressure of 10 Pa, and the plasma generator is ignited. Following this, the necessary gas pressure of the oxygen/nitrogen/argon mixture in the plasma generator is regulated to meet the required test conditions. As soon as a stable condition is achieved, the measurement equipment is activated, and the component is moved to its test position, enabling the commencement of the actual experiment.

The experiment will be concluded either after around 10 minutes, a steady state of the demise process is observed, or a complete decomposition of the component is achieved. The plasma generator will then be turned off and after a cooling down phase the vacuum chamber is vented.

Setup of the Sensor Validation Test

The validation of the re-entry sensors represents the second part of the PWK-test campaign.

As the SOURCE satellite is designed to carry out measurements during re-entry, the plasma wind tunnel can also be used in a non-destructive manner to validate the functionality of the sensor arrays under flight-like conditions and to ensure the sensors performance and on-board data acquisition capabilities. This is crucial for understanding the behavior of the sensors and their response times, which helps in characterizing the influence of tumbling and heat conduction during the actual re-entry. This test focuses on the re-entry sensors on the arrays around SOURCE and excludes FIPEX sensors, which require different test capabilities in a defined atomic oxygen environment.

For the sensor validation test, a mock-up of the SOURCE satellite was built on a 1:1 scale. It consists of the primary structure of the satellite, the re-entry sensor arrays, and the payload boards to power and read out these sensors. On Array 1, the PHLUX sensor is not operational, and on Array 5, the pressure sensor is not operational, both due to manufacturing errors. The rest of the model was completed by adding thermal models inside the satellite mock-up to ensure thermal comparability. The mock-up is mounted with the IRAS MSS side on a stepper motor, enabling rotation around the z-axis. The stepper motor is then mounted on the 4-axis CNC table. In the starting position of the mock-up ($\alpha = 0°$), Arrays 2 and 4 are facing towards the plasma generator nozzle and Array 3 is parallel to the plasma beam. The array positioning in relation to the plasma can be seen in Figure 12.

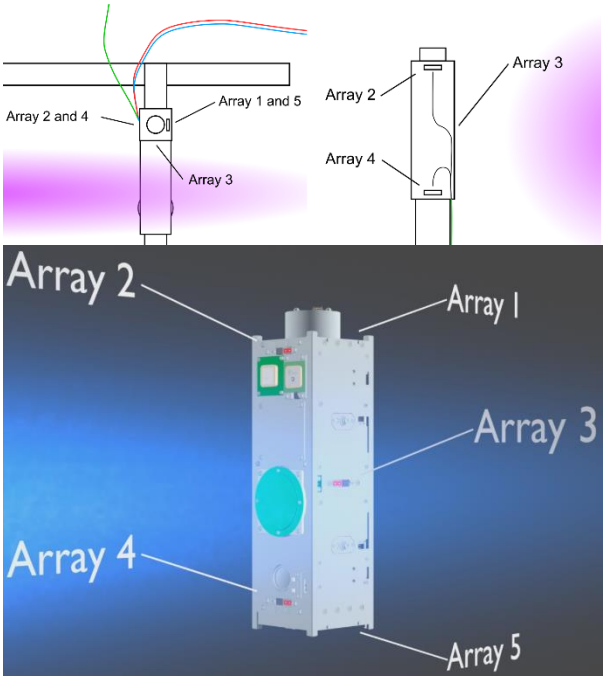

Figure 12: Array positioning for α = 0° as top, front and three-dimensional view

The mounted mock-up on the stepper motor with attached cables can be seen in the Figure 13.

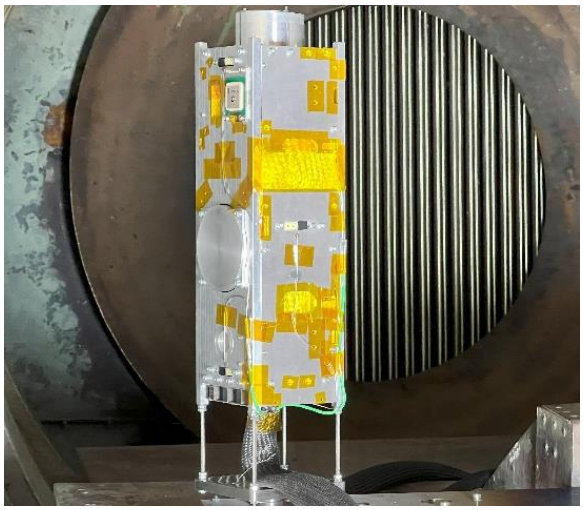

Figure 13: Mock-up of the SOURCE satellite in the plasma wind tunnel with Kapton tape to protect electronics from plasma flow

Data is collected via harness that is routed through the bottom of the model. The harness, along with cables for the thermocouples and the stepper motor, is shielded and directed through the bottom of the Plasma Wind Tunnel to the outside. For external measurements, four thermocouples are placed on the outside of the model in proximity to the sensor arrays for comparison; an additional one is placed on the inside near the payload board to ensure that data acquisition is not affected due to the circuitry exceeding its operational temperature range. This setup leaves Array 1 without a thermocouple, as the PWK1 has only 5 thermocouple channels. Additionally, a FLIR A6751sc SLS thermographic imaging camera is used to measure surface temperatures, and a 4K video camera is used to record the test, as it can be seen Figure 14.

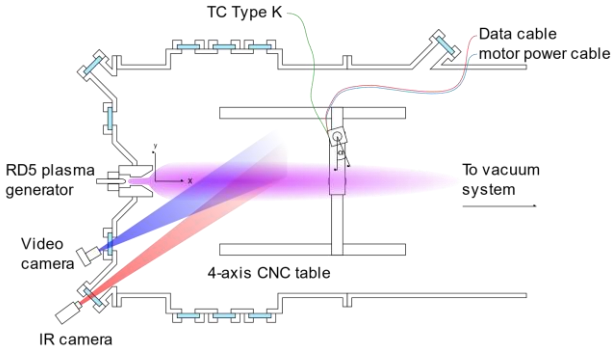

Figure 14: Sensor validation test setup as top view on the plasma wind tunnel

As this test is intended to be non-destructive, the plasma generator parameters are set significantly lower compared to those used in critical component testing. To further ensure lower heat flux on the mock-up, the test is conducted further away from the plasma generator and includes an offset towards the plasma beam, which brings it closer to the side walls of the plasma wind tunnel. Hence, compared to the critical component test where the components are directly in front of the generator, the mock-up only faces low amounts of plasma.

The sensor validation test operational parameters are based on previous simulations performed by PICLas, aiming to match the conditions as closely as possible.[40] The chosen operational Parameters are listed in Table 3.

Parameter	Symbol	Value
total gas mass flow	$\dot{m}$ [g/s]	2.3
Tank pressure	p_{Tank} [Pa]	10
Total pressure	p_{tot} [Pa]	45
Specific enthalpy (80mm ⌀ probe)	h [MJ/kg]	12.7
Generator current	I [A]	800
Generator voltage	U [V]	60
position	x [mm]	965

Table 3: Operational parameters for the sensor validation experiment

Due to the non-destructive nature of the test, it is repeated closer and closer to the plasma plume, ensuring that the sensors and circuitry are tested under increasing heat flux loads. The characterized test positions with an 80mm diameter heat flux probe can be seen in Table 4. The test was conducted at positions 1 and 2 fully, at positions 3 and 4 short static measurements were taken.

Parameter	Symbol	Value			
Test Position	-	1	2	3	4
Axial positions (distance to center)	y [mm]	640	540	490	440
heatflux density	$\dot{q}_{D=80\,mm}$ [kW/m^2]	1,4	2,2	2,2	3,1
total pressure	p_{tot} [Pa]	45	45	45	45

Table 4: Characterized test positions for the sensor validation experiment

To further simulate the re-entry of the satellite, the mock-up is rotated around the z-axis to simulate the tumbling of the satellite during re-entry. Based on the aerodynamic simulations, four different rotation speeds, 3.5, 5, 10, and 15 degrees per second, were selected to

cover the early phase of re-entry. This approach aims to measure the reaction time of the sensors and better understand the impact of tumbling on the data acquisition.[29]

Procedure Sensor Validation Test

After mounting the mock-up, the tank is closed, and data collection is started. The vacuum pumps are activated and after a stable vacuum is achieved, the plasma is ignited. Following ignition, the flow parameters for the gas is set to match the desired environment. After a steady plasma plume is created, the test is started. It begins with a static measurement at $\alpha = 0°$ for at least 30 seconds.

Afterwards, the rotation sequence is started. It begins with a rotation of 3.5 degrees per second to $\alpha = 360°$, followed by 30 seconds of static measurement. The rotation speed is then increased to 5 degrees per second back to $\alpha = 0°$, followed by 30 seconds of static measurement. This is then repeated with a rotation speed of 10 and 15 degrees per second. The back-and-forth rotation is necessary as the harness prevents the mock-up from rotating multiple times in the same direction.

The test is concluded after the last rotation and the plasma is turned off. Then, vacuum pumps are deactivated, and the tank is repressurized. Finally, the data collection is stopped.

EXPERIMENTAL RESULTS

The following section gives an overview on the preliminary experimental results of the critical component investigation and re-entry sensor validation.

Critical Component Results

The critical components experiments should be a first step toward an evaluation of the demisability of hard-to-demise CubeSat components, while also providing a reference point for the scarab simulations. Each component is looked at individually in the following section regarding visual and thermal inspections.[41]

Battery

The Battery consists of eight Li-Ion cells on an electric circuit board for housekeeping and heater control. It is surrounded by an aluminum structure holding the cells in place. To avoid a drop of the specimen in the first minutes due to the relative low melting point of aluminum, a stainless-steel holding cage was designed. This proved necessary for the test in the SRC-Med regime, as the aluminum structure demised completely in the first two minutes of the test. During the test, the maximum temperature was close to 1700 K, leading to an ejection of material from the cells most likely via theirs vents. However, the cells stayed, together with their PCB, mostly intact, which can be seen in Figure 15. The duration of the test was 12 minutes.

Figure 15: Battery before and after the 720 seconds test in the plasma wind tunnel with SRC-Med parameters

S-Band Antenna

The S-Band antenna from Anywaves consists of an aluminum housing and a cover made of Vespel, which is a polyamide. In the beginning of the test, the thin aluminum cover got brittle, and cracks started appearing on the surface. This led to the loss of the structural integrity, which caused the antenna to drop off the probe shortly after 4 minutes. The temperatures observed were in the range of 1400 K, which was expected for the SRC-Ant environment. In the end, the cylindrical shape is no longer recognizable, with the aluminum housing almost completely melted, leaving just dust-like fragments, as can be seen in Figure 16.

Figure 16: S-Band antenna before and after the 270 seconds test in the plasma wind tunnel with SRC-Ant parameters

IRAS-MSS

Located at one end of the satellite, the composite sandwich from the IRAS project, which consists of two carbon fiber-reinforced plastic layers (CFRP) and a polyether ether ketone (PEEK) honeycomb structure reinforced with short carbon fibers is equipped with embedded sensors. It was tested at a higher heat flux regime (SRC-Rod) than it was simulated with SCARAB due to experiences with demise-resistant CFRPs in plasma wind tunnel tests before. During the 10-minute experiment, the sandwich decomposed layer by layer, completely removing the top carbon plate as can be seen in Figure 17.

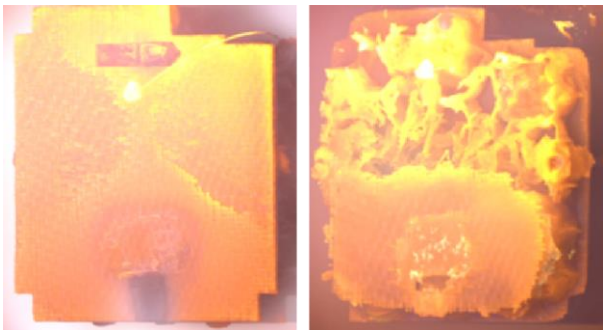

Figure 17: IRAS-MSS at 110 and 555 seconds after its critical component test start

On the sides, chunks of burnt material accumulated. The second plate of the CFRP frayed out and showed burn marks in the middle, where the components are located. However, the PEEK honeycomb structure proofed hard-to-demise as well, slowing down the disintegration of the second CFRP. Overall, the whole sandwich showed signs of deformation, as the back layer also bent from the thermal load and the honeycomb structure lost depth, as it is shown in Figure 18. However, even after 10 minutes in the high heat flux environment facing temperatures over 1800 K, a lot of the IRAS MSS survived.

Figure 18: IRAS-MSS before and after (side and front view) the 600 seconds plasma wind tunnel test with SRC-Rod parameters

Payload-PCBs

The two stacked payload PCBs consist mainly of fiberglass-reinforced plastic, copper and different kinds of plastic. The plasma wind tunnel tests were conducted at the SRC-Rod conditions for 6 minutes. It started decomposing losing connectors and chips from the surface from the early beginning. Moreover, it bent forward, towards the plasma generator. This transited in a stationary ablation process, resulting in the surface melting significantly and becoming flat again. Big droplets formed at the front and proceeded to follow the plasma plume. Excerpts of this process can be seen in Figure 19.

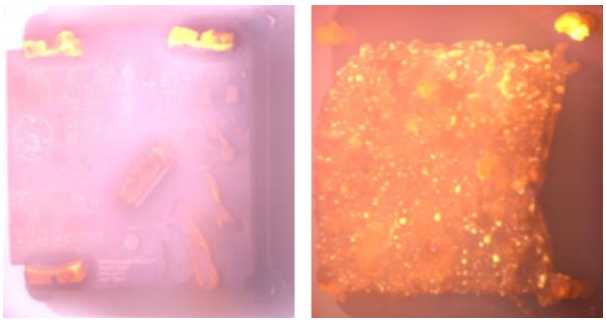

Figure 19: Payload PCBs at 1 and 350 seconds after its critical component test start

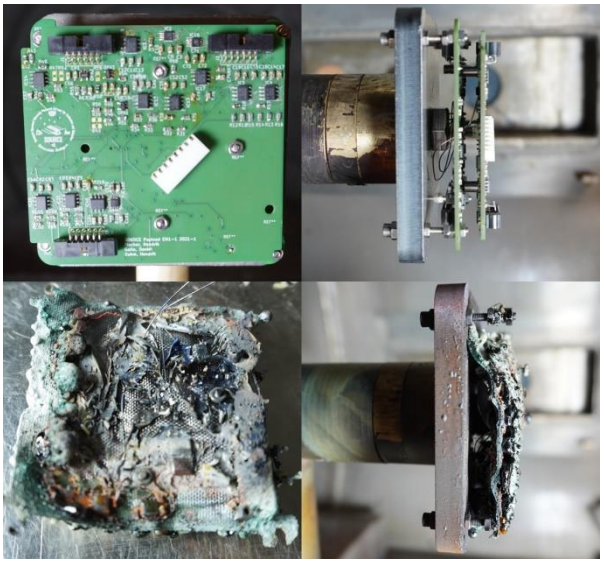

Figure 20: Payload PCBs before and after the 360 seconds plasma wind tunnel test with SRC-Rod parameters

After 5 minutes, processes stalled, and the experiment was concluded. After the test, the front circuit board deformed with a resolidified grey-green surface and clumped with the rear circuit board, which can be seen

in Figure 20. This makes it more difficult for any decomposition to take place during re-entry of this component.

Magnetorquers

SOURCE uses three magnetorquers consisting of a copper coil wound around a ferrite core. One of them was tested in the plasma wind tunnel with SRC-Med conditions for 10 minutes. Three minutes after ignition the copper wires were completely melted, and the ferrite core lost its cylindrical shape. Bubbles formed on the surface of the magnetorquer. The plasma plume's color changed to green due to the excitation of the copper atoms. After the copper was gone, a steady state was reached for the remaining 6 minutes. In the end, the temperature reached 1800 K, slightly melting the ferrite core. Its remains can be seen in Figure 21.

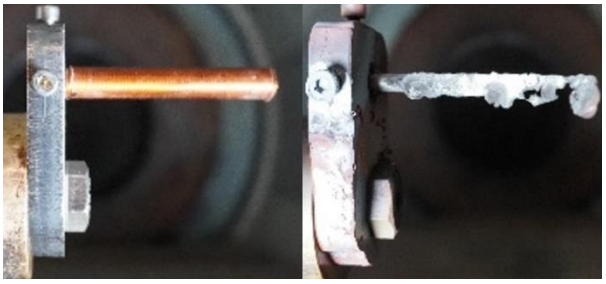

Figure 21: Magnetorquers before and after the 600 seconds plasma wind tunnel test in the SRC-Med condition

MeSHCam

The MeSHCam consists of an aluminum housing for mounting and a lens with a stainless-steel ring. It underwent two rounds of testing. During the first test, the entire MeSHCam assembly was evaluated in SRC-Med conditions. It was mounted in such a way that, after a minute of testing, partial melting of an aluminum component led to a loss of its structural integrity. This caused the optics to drop and shatter into several large pieces on the ground, which can be seen in Figure 22.

The second test focused on the lens, which stayed mostly intact after the first test's drop. During the second test with SRC-Rod conditions, the lens completely disintegrated. The melting of the optical system causing bubbles to surface during the 30 seconds test until the melting of the structural parts caused the front together with the lens to detach and fall onto the base plate, while the shutters remained on the mount and completely decomposed as it can be seen in Figure 23.

Figure 22: MeSHCam before and after 60 seconds of the plasma wind tunnel test with SRC-Med parameters

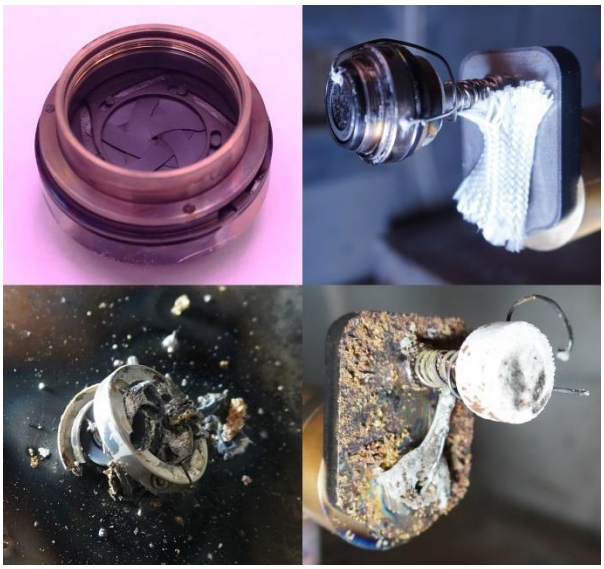

Figure 23: MeSHCam lens before (top) and after (bottom) the 30 seconds plasma wind tunnel test with SRC-Rod parameters

Titanium threaded Rods

SOURCE uses M3 threaded rods made of titanium in the longitudinal axis of the satellite to stack components with enough stiffness to survive the launch. During the high heat flux tests with SRC-Rod conditions for around 5 minutes, the titanium rod's temperature rose quickly to 1900 K, then dropped to 1700 K due to emissivity changes. The rod bend, causing asymmetric loading. The stainless-steel holder glowed and melted, detaching the top side of the rod. Temperature fluctuations and radiation color changes occurred, with the temperature rising to 2200 K due to bending and surface changes, showing greenish flames, most likely from vanadium. The temperature later reached 2500 K and deformation slows, forming a new stagnation point. After 4 minutes, a steady state was reached, and the rod stayed like it is depicted in Figure 24.

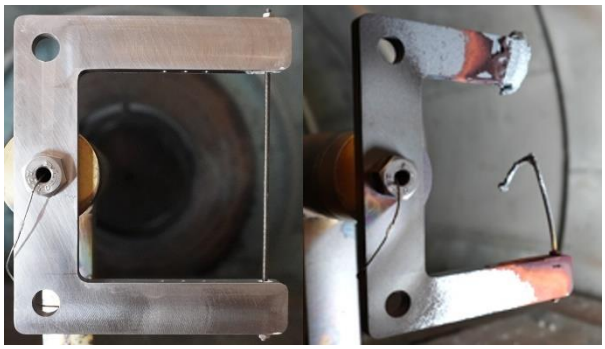

Figure 24: Titanium threaded rod before and after the 300 seconds plasma wind tunnel test with SRC-Rod parameters

Comparison to the SCARAB simulation

The results of the SCARAB simulation compared to the experimental tests for different satellite components show varying degrees of agreement.

For the S-Band Antenna, the experiment's conditions showed a very good compliance with the simulation, the highest deviation occurs in total pressure with 10 %. The component mostly disintegrated after 350 seconds in the simulation, while the test indicated earlier disintegration at 273 seconds, showing an overall satisfying accordance. The IRAS MSS demonstrated significant deviations in total enthalpy and total pressure, both over 35 %. The simulation predicted complete disintegration within 40 seconds, contrasting with the experimental partially disintegration time of 595 seconds, indicating poor agreement and suggesting the need for material property adjustments in the simulation. For the Payload PCB, the total enthalpy was 3 % and the temperature 2.9 % off the simulation, which indicates suitable experiment parameters. However, a complete disintegration as it was calculated in the simulation was not seen in the plasma wind tunnel experiments, indicating the need for further adjustments in material properties and recalibration of expected heat flux in the experiment to achieve a better compliance. The same can be said about the Batterie experiment, where parameters from the experiment only had minor deviations from the simulation but the demise process differed significantly. The Magnetorquer showed a 12 % deviation in total enthalpy, and a low deviation in temperature. The simulation predicted a shorter disintegration time (140 seconds) compared to the experiment (190 seconds). Despite this, there was a reasonable qualitative agreement regarding the structural integrity. For the MeSHCam, the parameters were 3.9 % in total enthalpy, 9.7 % in total pressure, 16.6 % in heat flux, and 2.4 % in temperature off compared to the simulations. Despite an early test termination, the results indicated a good overall agreement, with most of the structure disintegrating. Lastly, the Titanium Threaded Rod showed good agreement to SCARAB's calculation as well, as the component's survival in both simulation and experiment was predicted.

Sensor Validation Results

In this section, the results of the sensor validation test are presented and discussed. The purpose of the test was to recreate the initial stages of the re-entry phase in a controlled environment, allowing for the evaluation of the re-entry sensors' functionality.

Tests overall

The mock-up rotated as intended, and the data was collected. Figure 25 shows the mock-up during the test.

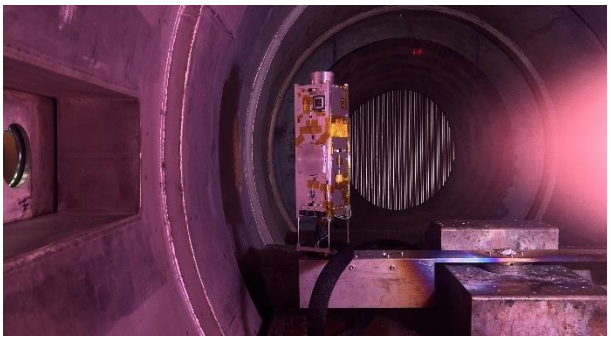

Figure 25: SOURCE mock-up during the sensor validation test

As the test was meant to be non-destructive, the mock-up was still in good condition afterwards, with no visible damage to the mock-up or the sensors. The sensors were also functionally tested after and showed no signs of malfunction. A thermal image after the sensor validation testing is shown in Figure 26. In this picture, the Kapton tape used to prevent the plasma from flowing inside the mock-up can be seen as rectangular stripes.

Sensor data

As mentioned in section Re-entry Sensor System, each sensor array consists of 3 sensors, measuring the heat flux density, temperature, and pressure. In the following, an overview of the collected data is presented and discussed. This work will mostly cover the data from the first test run to keep the analysis concise.

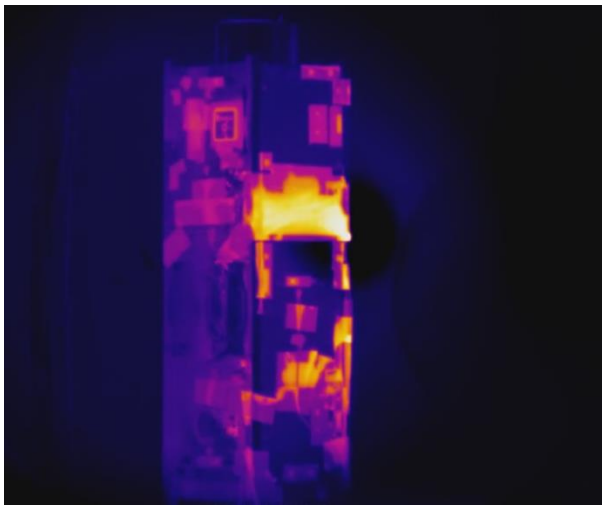

Figure 26: Thermal image of the satellite mock-up after the sensor validation test

Wuntronic FM-120-K

The Wuntronic FM-120-K sensor measures heat flux density and temperature. The measurement of the heat flux density for the first test of Array 2 can be seen in Figure 27. It should be noted that for the heat flux diagrams, the time from 100 s to 400 s has been compressed because the plasma was configured in this time and to highlight the visible rotations in the heat flux.

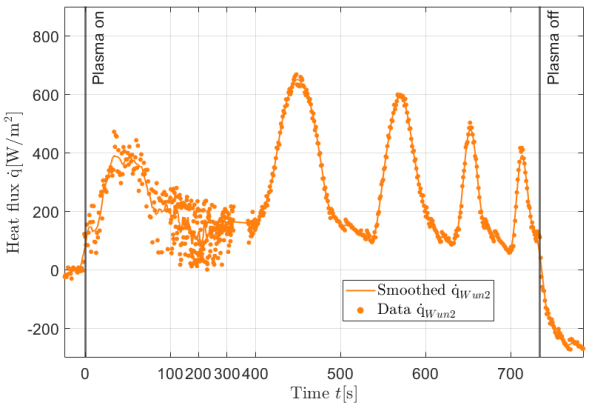

Figure 27: Heat flux density by the Wuntronic FM-120-K on Array 2

Overall, the FM-120-K sensor showed decent results concerning heat flux density. The sensors could identify high and low heat flux density areas, which is expected due to the rotation of the mock-up. When comparing Array 2 and Array 4, both positioned at the front of the plasma wind tunnel at $\alpha = 0°$, to the measuring probe, significant deviations were observed in the FM-120-K sensor readings. The 80 mm calibration probe measured 1400 W/m², while Array 2 measured an average of 141.6 W/m² and Array 4 measured an average of 23.2 W/m². However, it is important to note that Arrays 2 and 4 are not at the same z-axis position as the measuring probe. The probe was roughly at a height of 25 cm, resulting in a difference of ±15 cm, placing it in the middle of Arrays 2 and 4, which can explain the discrepancies. Especially since the plume of the plasma generator has a diameter for homogenous enthalpy distribution of approximate 10 cm. While the absolute values may not be accurate, the qualitative behavior can be evaluated by comparing the rate of temperature change recorded by the thermocouples positioned on each array to the heat flux density of the FM-120-K. An example comparison using Array 3's data from the first test run is displayed in in Figure 28.

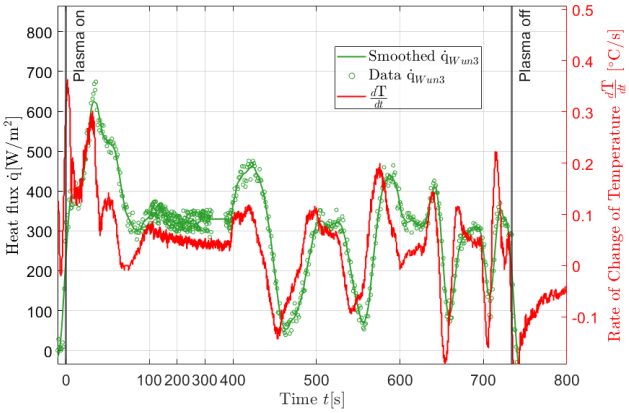

Figure 28: Heat flux density and temperature change rate as recorded by sensor Array 3 in the first sensor validation test run

As the heat flux density increases, the wall temperature is expected to rise accordingly, which is consistent with the observed data. In the second test run, the heat flux density data from the FM-120-K sensors exhibited significant scatter across almost all arrays, with only Array 3 providing plausible data. The reason for this discrepancy is not yet clear.

The secondary measurement of the FM-120-K is temperature, as illustrated in Figure 29. For comparison, a calibrated thermocouple glued next to the sensor array is displayed as well. The comparison of the temperature measurements of the Wuntronic FM-120-K sensor to the thermocouples shows a significant deviation. While the trend is similar, the absolute values are off by a substantial amount. It is noteworthy that following plasma ignition and shutdown, the thermocouple exhibited an immediate response. In contrast, the FM-120-K took over 200 seconds to register an increase in

temperature. This data also suggests that the absolute value of the measured heat flux density needs to be adjusted, as the temperature is used to derive the heat flux density. In the second test run, the problems with the temperature measurements persisted.

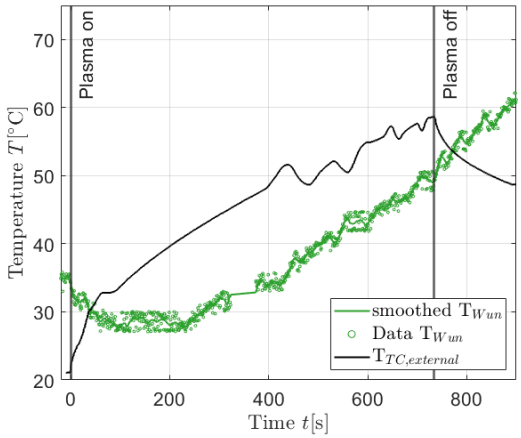

Figure 29: Temperature measurement comparison between the Wuntronic FM-120-K on Array 3 and a thermocouple in close vicinity

PHLUX

As the basis for the chemical heat flux and atomic oxygen measurement, the PHLUX sensor system utilizes two temperature sensors, as explained in the Re-entry Sensor System section. The sensor validation test helps to understand accuracy and quality of the sensor suit and gives a first insight into next calibration steps.

The test demonstrated that the used PT-1000 sensors showed standard performance, as the measured temperature course is almost identical to the temperature measured by the thermocouples. An offset of a few Kelvins, as depicted in Figure 30, was observed. This is the case for all four functioning PHLUX sensors in both tests. The exception is Array 4, where the PHLUX sensor failed and one of the PT 1000's consistently read 550 °C after a few minutes. Regarding the temperature differences within each sensor's differently coated PT1000, the results varied between the arrays. First, even in the absence of any plasma there is a slight temperature difference between the coated and un-coated sensor. Therefore, only a meaningful difference in temperature can be attributed to plasma and the recombination of the atomic oxygen during the test. For Array 5, mounted at the bottom of the mock-up, the temperature difference during the test runs is similar to the condition with no plasma exposure. This is expected, since this array is furthest away from the plasma plume. For Arrays 2 and 3, the temperature difference between the coated and un-coated sensor increases with the plasma exposure, which is anticipated, as seen in Figure 31. The depicted temperature difference shows the adjusted values with the baseline difference between the two sensors removed, highlighting only the difference caused by a possible recombination. Array 4 showed similar behavior to Array 2 and 3 but failed during the test, so the data is not as conclusive.

A complete analysis of the measurement data must be conducted in the future in order to determine atomic oxygen fluxes in the plasma wind tunnel flow.

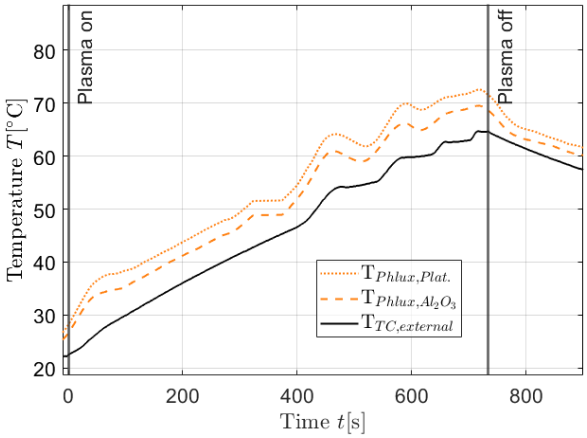

Figure 30: Array 2's PHLUX sensor temperature measurements in comparison with a thermocouple in close vicinity

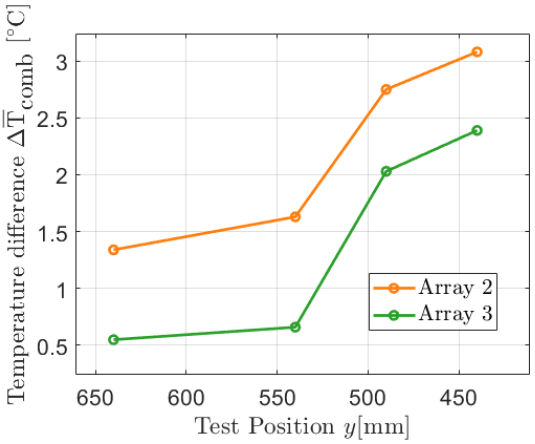

Figure 31: Temperature difference between Pt coated and Al2O3 coated PT1000 in the PHLUX sensors of Array 2 and 3 at different y positions

PVC1004 pressure sensor

The pressure measurement of the PVC1004 shows qualitative agreement with the inbuilt pressure sensor of

the plasma wind tunnel, with an offset of around 20 Pa. It clearly displays the most drastic pressure changes, such as at the end of the test when the gas flow is stopped or when the tank is repressurized. However, the sensor could not detect nuanced pressure changes during the rotation of the mock-up, which was also observed in the second test run. This can be seen in Figure 32 for Array 3 in the first test run.

Further calibration runs in a very low vacuum environment at different sensor temperatures might increase the achieved accuracy. Hence, the data need to be analyzed further.

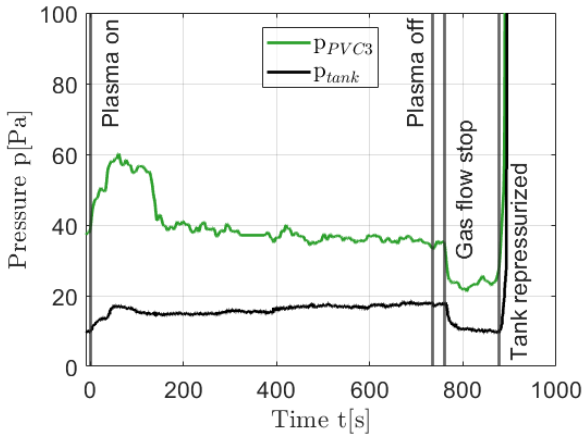

Figure 32: Pressure measurement of the PVC1004 on Array 3 and the plasma wind tunnel's integrated pressure sensor

Sensor Validation Test Comparison with Simulations

In the following section, the sensor results from the first test run of the sensor validation test are compared to the PICLas simulations of the re-entry of the SOURCE satellite.[40]

This comparison comes with challenges due to the limited altitude conditions of the test, which differ from the tumbling experienced during an actual re-entry scenario. While this difference can be accommodated in heat flux measurements, it requires careful consideration for temperature measurements, as temperatures rise progressively until equilibrium is achieved, resulting in significantly higher final temperatures. Additionally, the mock-up was positioned in close proximity to, rather than directly within, the plasma. Consequently, the simulation and the real satellite encounter distinct flow conditions, leading to variations in plasma dynamics.

The simulation was conducted from 200 km to 130 km for two kinds of atmospheres: a hot and a cold case. These cases refer to the highest and lowest expected atmospheric densities and solar activities during re-entry. The relevant results are depicted in Table 5.

Parameter	Symbol	Cold case		Hot case	
Altitude	h[km]	140	130	140	130
Maximum heat flux density	$\dot{q}$[W/m^2]	600	1100	1100	2200
Wall temperature	T_W [°C]	-10	18	20	55
Maximum pressure	p[Pa]	0,2	0,3	0,3	0,6

Table 5: Results of the PICLas simulations[40]

As mentioned in the Wuntronic FM-120-K results section, the deviations between arrays and the heat flux probe are approximately a factor of 10. This discrepancy is also observed when comparing the sensor data to the simulations, as the plasma wind tunnel conditions were based on them. The first test position was characterized to match the conditions for the hot case at 140 km or the cold case at 130 km. The heat flux of an array exposed to plasma was computed to be approximately 1100 W/m², but only an average of 141.6 W/m² was measured on Array 2, which was facing towards the plasma generator nozzle. Even if the FM-120-K measurement is taken at face value, with a maximum of 670 W/m² being measured in the first test position, this would correspond to the hot case at 150 km and the cold case at 140 km. This necessitates further work to ensure that measurements in space will be accurate. The temperature measurements did not reach a significant equilibrium; it continuously increased until the plasma was turned off. At the end of the test, the wall temperature, measured by externally attached thermocouples, stabilized between 50 °C and 65 °C, which is warmer than the expected temperature of around 20 °C, for both comparison scenarios. This discrepancy is likely due to prolonged exposure to the simulated conditions and the initial temperature of around 20 °C at the start of the test.

The pressure data has several limitations. Firstly, the vacuum system of PWK1 is incapable of achieving the low pressures required to replicate the simulations accurately. Additionally, the selected sensors are known to have suboptimal performance for this use case. The simulated pressure is between 0,2 Pa and 0,6 Pa, which is a significant difference to the sensor data settled at 40 Pa. The computed pressures also reveal a clear distinction between exposed and less exposed arrays, with increased exposure correlating to higher pressure. This behavior could not be observed in the test.

CONCLUSION AND OUTLOOK

A short overview of the interdisciplinary approach on satellite demisability at the University of Stuttgart was given in the introduction. Embedded in this, SOURCE's satellite bus was presented with a focus on its measurement suit for satellite re-entry investigation. This was followed by the description of conducted plasma wind tunnel experiments, which has provided significant insights and identified areas for further research in satellite re-entry investigation. The SCARAB simulations demonstrated good agreement with the experimental results for most components, such as the S-Band antenna, titanium rods, and the MeSHCam, indicating the robustness of the simulation tool for predicting re-entry behavior. However, deviations observed for components like the Payload PCBs and CFRP structures underlines the need for refined material properties in simulations to enhance prediction accuracy. The sensor validation test, using a mock-up of the SOURCE satellite, showed promising preliminary results. The mock-up's sensors performed as expected under the simulated conditions, showing the capability of capturing relevant in-situ data during early phase of re-entry.

Future work will focus on additional plasma wind tunnel tests to improve the SCARAB model, particularly for hard-to-demise components such as PCBs and CFRP structures. These efforts will be critical in enhancing the accuracy of component demise models. Moreover, investigation on the scalability of results will be pursued to connect CubeSat component demisability to small satellites re-entries in general. Additional tests with the SOURCE mock-up are discussed to improve sensor accuracy.

In summary, the interdisciplinary approach, which combines numerical simulations, plasma wind tunnel experiments, and in-situ sensor validation, is proving effective in advancing the understanding of satellite re-entry dynamics. It will help address the challenges of space debris and ensure the long-term sustainability of low Earth orbit operations with improved predictions and best practice advice.

ACKNOWLEDGEMENTS

This paper was made possible by the effort and enthusiasm of the SOURCE team which includes students from KSat e.V. and staff from IRS with their incredible work and dedication for this CubeSat project. The team further expresses their gratitude to Hyperschall Technologie Göttingen (HTG) for their very generous and extensive support of this research activity. The project is funded by the Federal Ministry for Economic Affairs and Climate Protection based on a resolution of the German Bundestag. SOURCE is additionally supported by ESA's 'Fly Your Satellite!' program with test facilities and experts.

References

1. ESA, "ESA'S ANNUAL SPACE ENVIRONMENT REPORT", https://www.sdo.esoc.esa.int/environment_report/Space_Environment_Report_latest.pdf, 2023
2. Langer, M. and Bouwmeester, J., "Reliability of CubeSats – Statistical Data, Developers' Beliefs and the Way Forward", Proceedings of the AIAA/USU Conference on Small Satellites, SSC16-X-2, August 2016.
3. NASA, "Orbital Debris Quarterly News", Volume 28, Issue 1, February 2024.
4. ESA Space Debris Mitigation Working Group, "ESA Space Debris Mitigation Requirements", ESSB-ST-U-007 Issue 1, October 2023.
5. PICLas Developers, "PICLas Documentation", 2021.
6. Koppenwallner, G., Fritsche, B. and Lips, T., "SCARAB - A Multi-Disciplinary Code for Deconstruction Analysis of Space-Craft During Re-entry", ESA SP-563, Cologne, Germany, Nov. 2005.
7. Pagan, A. S., Massuti-Ballester, B., Herdrich, G., Merrifield, J. A., Beck, J. C., Liedtke, V. and Bonvoisin, B., "Experimental Investigation of Material Demisability in Uncontrolled Earth Re-entries", 31st International Symposium on Space Technology and Science, Matsuyama, Japan, 2017.
8. Pagan, A.S. and Herdrich, G., "Key parameters governing the ground risk from reentering pressure vessel debris", JSSE., 9 (2022), pp. 189–200.
9. Bonvoisin, B., Meisnar, M., Merrifield, J., Beck, J., Lips, T., Guelhan, A., Schleutker, T., Herdrich, G., Pagan, A., Kaschnitz, E., Liedtke, V., Helber, B., Lopes, S., Gouriet, J. B., Chazot, O. and Ghidini, T., "Demisability assessment of space materials", CEAS Space Journal., 15 (2023), pp. 213–235.
10. Beck, J., Caiazzo, A., Gülhan, A., Innocenti, L., Schleutker, T. and Soares, T., "Plasma Wind Tunnel Demisability Testing of Spacecraft Equipment", International Orbital Debris Conference 2019, Sugar Land, Texas, USA, IOC Paper 2019-6107, 2019.
11. Löhle, S., Zander, F., Lemmens, S. and Krag, H., "AIRBORNE OBSERVATIONS OF RE-ENTRY BREAK-UP: RESULTS AND PROSPECTS", Proc. 7th European Conference on Space Debris, Darmstadt, Germany, April 2017

12. Pasquale, E. de, Francillout, L., Wasbauer, J.-J., Hatton, J., Albers, J. and Steele, D., "ATV Jules Verne reentry observation: Mission design and trajectory analysis", 2009 IEEE Aerospace conference, Big Sky, MT, USA, AERO.2009.4839703, 2009.
13. Dumon, J., Constant, E., Spel, M., Lips, T., Kanzler, R., Pagan, A., Buntz, M., Herdrich, G., Santana, C., Sanvido, S., Lemmens, S. and Annaloro, J., "Rebuild and data exploitation of the AVUM re-entry event for break-up model development", 2nd International Conference on Flight Vehicles, Aerothermodynamics and Re-entry Missions & Engineering (FAR), Heilbronn, Germany, 2022.
14. Kissel, G., Loehrlein, R., Kalsch, N., Helms, W., Snyder, Z. and Kaphle, S., "UNITE CubeSat: From Inception to Early Orbital Operations", 33rd Annual AIAA/USU Conference on Small Satellites, U.S.A., Logan, 2019.
15. Prevereaud, Y., Sourgen, F., Mimoun, D., Gaboriaud, A., Verant, J. L. and Moschetta, J. M., "Predicting the Atmospheric Re-entry of Space Debris Through the QB50 EntrySat Mission", 6th European Conference on Space Debris, Darmstadt, 2013.
16. Zuiker, N. J., Williams, J., Putnam, Z. R., Levin, D. A., Ghosh, A., Goggin, M. and Alexeenko A., "Design of a CubeSat Mission to Investigate High-Enthalpy Nonequilibrium Flow Chemistry", AIAA Aerospace Sciences Meeting, U.S.A., Kissimmee, 2018.
17. Krebs, Gunter D., „SASSI2", Gunter's Space Page, Retrieved June 05, 2024, from https://space.skyrocket.de/doc_sdat/sassi2.htm
18. Denis, A., Umit, E., Le Quang, D., Van Der Haegen, V., Magin, T., and Chazot, O., „QARMAN: POST-FLIGHT MISSION OVERVIEW, DATA ANALYSIS, AND LESSONS LEARNED FROM VKI RE-ENTRY CUBESAT", The 4S Symposium 2022
19. Nagata, Y., Yamada, K., Suzuki, K. and Imamura, O.: Flight Demonstration of Telecommunication System for Satellite using Iridium Communication, Journal of the Japan Society for Aeronautical Space Science, 67 (2019), pp. 1-6.
20. JAXA, "Two CubeSats successfully deployed from 'Kibo'!", Announcement, December 2023.
21. Graduate School of Frontier Sciences of The University of Tokyo, "REACHING SPACE FROM KASHIWA", SOSEI 39, 2022.
22. Stier, A., Schweigert, R., Galla, D., Lengowski, M. and Klinkner, S., "Combination of Interdisciplinary Training in Space Technology with Project-Related Work through the CubeSat SOURCE", 3rd Symposium on Space Educational Activities, Leicester, United Kingdom, September 2019.
23. Baetz, B., Mohr, U., Klemich, K., Bucher, N., Klinkner, S. and Eickhoff, J., "The flight software of Flying Laptop: Basis for a reusable spacecraft component framework", IAA Symposium, Berlin, Germany, April 2017
24. Koller, M., Bötsch-Zavřel, L., Eggert, M., Fugmann, M., Holeczek, C., Kranz, M., Lengowski, M., Löffler, T., Loidold, L.-M., Maier, P., Meier, J., Mohr, U., Müller, R., Pahler, A., Pätschke, S., Schweigert, R., Starzmann, D., Steinert, M., Zietz, M. and Klinkner, S., "Lessons Learned and First Results of the E-Band CubeSat EIVE", 10.21203/rs.3.rs-3748010/v1, December 2023
25. Petri, J., Klinkner, S. and Zink, J., "Hardware accelerated onboard image processing for space-based meteor observation - Concept and Implementation of SpaceMEDAL", 4S Symposium, Vilamoura, Portugal, 2022
26. Hümbert, S., Meth, J., Echsel, M., Lengowski, M. and Stäbler, T., "Additive manufacturing of radiation shielding for small satellites", 72nd International Astronautical Congress (IAC), October 2021
27. Eberhart, M., Lohle S., Steinbeck, A., Binder, T. and Fasoulas, S., "Measurement of atomic oxygen in the middle atmosphere using solid electrolyte sensors and catalytic probes", Atmospheric Measurement Techniques, 8, 3701–3714, https://doi.org/10.5194/amt-8-3701-2015, September 2015.
28. Galla, D., Fischer, H., Haufe, P. J., Herdrich, G., Kaiser, C., & Klinkner, S. (2022, June). In-situ measurements in early phase re-entry of the source cubesat for numerical simulation validation. In 2nd International Conference on Flight Vehicles, Aerothermodynamics and Re-entry Missions & Engineering (FAR), Heilbronn, Germany.
29. Vorago 10820 Datasheet, https://www.voragotech.com/products/va10820 (accessed June 06, 2024)
30. Galla, D., Klinkner, S., Herdrich, G. et al., "The Educational Platform SOURCE - A CubeSat Mission on Demise Investigation Using In-Situ Heat Flux Measurements", 70th International Astronautical Congress, Washington D.C., USA, September 2019.
31. PVC1000 Series Datasheet, https://posifatech.com/wp-content/uploads/2019/03/Datasheet_PVC1000_PiraniVacuum_RevC_C1_120.pdf (accessed June 06, 2024)

32. FM-120-K Datasheet, https://www.wuntronic.de/en/Miniature-Heat-Flux-Sensors.html?file=files/wuntronic-theme-2016/Downloads/Miniature_heat_flux_eng.pdf (accessed June 06, 2024)
33. Steinbeck, A., “Methode zur Messung von atomaren Sauerstoff mittels katalytischem Prinzip”, Ph.D. thesis, University of Stuttgart, 2016 (German).
34. Lein, S., Steinbeck, A., Preci, A., Fertig, M., Herdrich, G. and Röser, H. and Auweter-Kurtz, M., “Final Design and Performance Parameters of the Payloads PYREX, PHLUX and RESPECT on EXPERT”, Transactions of the Japan Society for Aeronautical and Space Sciences, Aerospace Technology Japan, 8, ISTS27 (2010), pp. Tm 41–Tm 47.
35. Galla D., Klinkner, S., Herdrich, G., Kaiser, C., Kuhm, H. and Fischer, H.: The Detailed Design of the SOURCE Satellite for Demise Investigation, 33rd International Symposium on Space Technology and Science, Oita, Japan, February 2022.
36. Pagan A., Herdrich G.: Empirical Extraction of Quantitative Material Demisability Parameters from Plasma Wind Tunnel Experiments, 2nd International Conference on Flight Vehicles, Aerothermodynamics and Re-entry Missions & Engineering (FAR), 2022
37. Galla, D., Kaiser, C. F., Haufe, P. J., Hoffmann, P., O’Donohue, M., Hufgard, F., Dürnhofer, C., Pagan, A. S., Löhle, S., Herdrich, G. and Klinkner, S., "Demise Instrumentation Verification of the CubeSat SOURCE with End-to-End Plasma Wind Tunnel Experiments," 34th International Symposium on Space Technology and Science, Kurume, Japan, 2023.
38. HTG GmbH, "SCARAB: SpaceCraft Atmospheric Re-entry and Aerothermal Break-up," [Online]. Available: https://www.htg-gmbh.com/en/htg-gmbh/software/scarab/. [Accessed: 25-Jun-2024].
39. ESA Space Debris Mitigation WG: ESA Space Debris Mitigation Compliance Verification Guidelines, ESSB-HB-U-002, Feb. 2023
40. Kaiser, C. F., "Numerical Simulation of the Rarefied, High-Enthalpy Gas Flow during Atmospheric Entry for SOURCE, a 3U CubeSat," Master's thesis, University of Stuttgart, Stuttgart, Germany, 2020.
41. Ahamed, I., "Investigation of the demise behavior of critical CubeSat components in a plasma wind tunnel," Bachelor's thesis, University of Stuttgart, Stuttgart, Germany, 2024.